

## SHORT COMMUNICATION

# Flame-retardant rigid polyurethane foam with a phosphorus-nitrogen single intumescent flame retardant

Chao Wang<sup>1</sup> | Yicheng Wu<sup>1</sup> | Yingchun Li<sup>1</sup> | Qian Shao<sup>2</sup> | Xingru Yan<sup>3</sup> | Cui Han<sup>2</sup> | Zhe Wang<sup>4</sup> | Zhen Liu<sup>5</sup> | Zhanhu Guo<sup>3</sup> 

<sup>1</sup>School of Materials Science and Engineering, North University of China, No. 3 Xueyuan Road, Taiyuan, Shanxi 030051, PR China

<sup>2</sup>College of Chemical and Environmental Engineering, Shandong University of Science and Technology, Qingdao, Shandong 266590, China

<sup>3</sup>Integrated Composites Laboratory, Department of Chemical and Biomolecular Engineering, University of Tennessee, Knoxville, Tennessee 37996, USA

<sup>4</sup>Department of Chemistry, Xavier University of Louisiana, New Orleans, Louisiana 70125, USA

<sup>5</sup>Department of Physics and Engineering, Frostburg State University, Frostburg, Maryland 21532, USA

## Correspondence

Chao Wang, School of Materials Science and Engineering, North University of China, No. 3 Xueyuan Road, Taiyuan, Shanxi 030051, PR China.

Email: wangchao\_nuc@126.com

Zhanhu Guo, Integrated Composites Laboratory, Department of Chemical and Biomolecular Engineering, University of Tennessee, Knoxville, TN 37996, USA.

Email: zguo10@utk.edu

## Funding information

National Natural Science Foundation of China, Grant/Award Number: 51603194; National Institute on Minority Health and Health Disparities, Grant/Award Number: 5G12MD007595, and 8UL1GM118967; North University of China; University of Tennessee

A phosphorous-nitrogen intumescent flame-retardant, 2,2-diethyl-1,3-propanediol phosphoryl melamine (DPPM), was synthesized and characterized by Fourier transform infrared spectroscopy and nuclear magnetic resonance. Flame-retardant rigid polyurethane foams (RPUFs) with DPPM (DPPM-RPUF) as fire-retardant additive were prepared. Scanning electron microscope (SEM) and mechanical performance testing showed that DPPM exhibited a favorable compatibility with RPUF and negligibly negative influence on the mechanical properties of RPUF. The flame retardancy of DPPM on RPUF was investigated by the limiting oxygen index (LOI), vertical burning test and cone calorimeter. The LOI of DPPM-RPUF could reach 29.5%, and a UL-94 V-0 rating was achieved, when the content of DPPM was 25 php. Furthermore, the DPPM-RPUF exhibited an outstanding water resistance that it could still obtain a V-0 rating after water soaking. Thermogravimetric analysis showed that the residual weight of RPUF was relatively low, while the charring ability of DPPM-RPUF was improved greatly. Real-time Fourier transform infrared spectroscopy was employed to study the thermo-oxidative degradation reactions of DPPM-RPUF. The results revealed that the flame-retardancy mechanism of DPPM in RPUF was based on the surface charred layer acting as a physical barrier, which slowed down the decomposition of RPUF and prevented the heat and mass transfer between the gas and the condensed phases.

## KEYWORDS

2,2-diethyl-1,3-propanediol phosphoryl melamine (DPPM), flame retardant, polyurethane foams

## 1 | INTRODUCTION

Rigid polyurethane foam (RPUF) has been widely used as insulating materials, construction panel sandwich structures, cushions of furniture and packaging materials in automobiles, transportation, energy storage and electromagnetic interference shielding fields due to its high mechanical properties, insulated properties, etc.<sup>1-4</sup> However, one of its major defects is its flammability, which limits its further

applications.<sup>5,6</sup> The improvement of the flame retardancy of RPUF has currently been an important subject among the developments of new polymer foam materials.<sup>7,8</sup> Traditionally, the main flame retardants for RPUF are the halogen-based compounds such as pentabromodiphenyl ether, chloroethylphosphate, etc, which may endow RPUF excellent flame retardation.<sup>9</sup> However, when burning, such retardants release a lot of toxic gases which pollute environment and damage people's health.<sup>10-14</sup> Thus, the environmentally-friendly

flame-retardant additives with good flame retardancy are particularly needed. In recent years, the phosphorus-nitrogen intumescent flame retardants (IFR) have been widely used as halogen-free additives because they provide excellent fire protection with less smoke and lower toxicity.<sup>15,16</sup> Traditional IFRs are mixtures, which usually consist of an acid source (eg, ammonium polyphosphate), a carbonizing agent (eg, pentaerythritol, sorbitol) and a foaming agent (eg, melamine). The IFRs system usually experiences an intense expansion and forms protective charred layers that serve as a physical barrier to protect the underlying material from flux or flame.<sup>14,15</sup> In spite of many advantages, IFRs have 2 issues, ie, low water solubility and high thermal stability.<sup>17</sup> In addition, they are poorly compatible with the RPUF matrix, which weakens the mechanical properties of the RPUF.<sup>18,19</sup>

In order to overcome the disadvantages of traditional IFR, the developed single IFR, which chemically combines the acid source, carbonization agent, and blowing agent into 1 molecule, plays a synergism among the 3 components.<sup>17</sup> They exhibit excellent flame retardancy and char-forming ability in many polymeric materials and have slight damage on the mechanical properties of polymeric matrix.<sup>20,21</sup> For example, Gao et al prepared flame-retardant RPUFs with macromolecular phosphorus-nitrogen single IFR (MIFR) and reported that the MIFR-filled RPUFs had a good flame retardancy.<sup>22</sup> When the content of MIFR was 25 (ph), the limiting oxygen index (LOI) of the RPUF reaches 24.5%, and the compressive strength of the flame-retardant RPUFs does not decrease dramatically compared with that of pure RPUFs. However, the MIFR is water soluble, and the flame-retardant composites are easily attacked by water and exuded, leading to a deterioration of the flame retardancy. A suitable flame retardant for RPUFs is needed to overcome the aforementioned problems.

Herein, a novel phosphorus-nitrogen single IFR, 2,2-diethyl-1,3-propanediol phosphoryl melamine (DPPM), was synthesized and used as a flame-retardant additive for RPUFs. The effects of DPPM on the compatibility with RPUF and the mechanical, water resistance as well as flame-retardant properties of RPUF were examined, and the flame-retardant mechanisms of DPPM in RPUF were also investigated.

## 2 | EXPERIMENTAL

### 2.1 | Materials

Triethylamine and melamine (MA) were obtained from Shanghai Lingfeng Chemical Plant. Polyether polyols 4110 (average functionality: 4.1; OH content: 450.0 mg KOH/g; viscosity: 3.283 Pa. s at 25 °C; number average molecular weight: 550 g mol<sup>-1</sup>) was obtained from Shanghai Gao Qiao Petro. Co. Surfactant polysiloxane-polyether copolymer: Tegostab B8469 (PSCT) was obtained from Shanghai Chemical Reagent Co., China. Catalyst (dibutyltin dilaurate [DBDT]) was obtained from Sichuan Chemical Reagent Co., China. 4,4'-Diphenylmethane diisocyanate (MDI, -NCO content by weight 30%, viscosity: 0.220 Pa. s at 25 °C) was purchased from Shandong Yantai Wanhua Polyurethane Co., China. All the starting materials

and solvents were commercially available and were used without further purification.

2,2-Dimethyl-1,3-propanediol phosphoryl chloride (DPPC) was synthesized according to the published procedures.<sup>23</sup> Briefly, The flask was charged with 30 mL dichloroethane and 2,2-diethyl-1,3-propanediol (0.1 mol). The mixture was stirred and heated. When the reaction temperature reached 55 °C, 9.6 mL POCl<sub>3</sub> was added within about 1.5 h. Thereafter, the mixture was heated to 83 °C and kept under reflux for approximately 3 h. The reaction was kept at the same temperature until no HCl released. Successively, the reaction mixture was cooled down slowly to room temperature and removed the dichloroethane solvent. The white solid was washed once with 30-mL hexane and twice with 30-mL ether. The powdery product was dried at 70 °C under vacuum to a constant weight.

### 2.2 | Synthesis of DPPM

MA (12.6 g, 0.1 mol) and triethylamine (10.1 g, 0.1 mol) were added into 200 mL dioxane and heated to 100 °C. And then, the DPPC (23.0 g, 0.1 mol) in dioxane (50 mL) was dropwise added into the solution under stirring and continued to be stirred for several hours. Successively, the reaction mixture was slowly cooled down to room temperature, and the dioxane solvent was removed by rotatory evaporator. The brown crude product was purified by recrystallization from dioxane and was dried under a vacuum until a constant weight was reached. The yield was approximately 73.3%, and the melting point (m.p.) was >250 °C. Scheme 1 shows the synthesis route.

### 2.3 | Preparation of flame-retardant RPUF with DPPM

The flame-retardant RPUF samples were prepared by the 1-pot method. Briefly, polyols 4110, distilled water, DBDT, trimethylamine, PSCT and DPPM were well mixed in a 1-L beaker. Next, MDI was added into the beaker with vigorous stirring. The mixtures were immediately poured into an open mold (300 × 200 × 150 mm<sup>3</sup>) to produce free-rise foam. The foam was cured for 168 h under ambient conditions. The formulations of flame-retardant RPUF were shown in Table 1.

### 2.4 | Characterizations

#### 2.4.1 | Structure characterization

Infrared spectroscopy (IR) was applied on a Vector-22 Fourier transform infrared (FTIR) spectroscopy spectrometer (Bruker, Germany) using KBr pellets. <sup>1</sup>H NMR spectrum was recorded on a Bruker AV II-400 MHz spectrometer (Bruker, Germany) using tetramethylsilane



**SCHEME 1** Synthesis of DPPM

**TABLE 1** Formulations of flame-retardant RPUF containing different DPPM contents

Material	pph <sup>a</sup>
Polyols 4110	100
DBDT	0.26
Triethylamine	0.46
PSCT	2.0
Distilled water	0.4
DPPM	0-25
MDI	150

<sup>a</sup>parts per hundred of polyol by weight.

(TMS) as a reference and DMSO-*d*<sub>6</sub> as a solvent. Elemental analysis was applied on a Vario EL III instrument (Germany).

#### 2.4.2 | LOI test

LOI test was performed using an HC-2 oxygen index test instrument (China) in terms of the standard LOI test, ASTM D 2863-97. The specimens for measurement were cut to a size of 127 × 10 × 10 mm<sup>3</sup>.

#### 2.4.3 | Vertical burning tests

The vertical burning tests were performed with a CZF-5 vertical burning instrument (China) according to ASTM D 3801-96. The specimens for measurement were machined into sheets with size of 127 × 13 × 10 mm<sup>3</sup>.

#### 2.4.4 | Thermogravimetric analysis

Thermogravimetric analysis (TGA) was carried out in a TG-209F3 thermal analyzer (Germany) at a scanning rate of 10 °C/min under N<sub>2</sub> gas. Four-milligram samples were heated under nitrogen from room temperature to 700 °C.

#### 2.4.5 | Scanning electron microscope analysis

The surface of residues of the flame-retardant RPUF was investigated with a SU-1500 scanning electronic microscopy (Japan). The residue samples for scanning electron microscope (SEM) observations were obtained after combustion in their limiting oxygen concentration. SEM images of the residual char samples were taken after coating a gold layer on their surfaces.

#### 2.4.6 | Cone calorimeter test

The cone calorimeter test was performed using a Stanton Redcroft cone calorimeter (America) under a heat flux of 50 kW/m<sup>2</sup> according to ISO-5660 standard procedures. The specimens for measurement were cut to a size of 100 × 100 × 10 mm<sup>3</sup>.

#### 2.4.7 | Compressive strength test

The compressive strength was measured by a universal electronic tensile machine (Shimadzu, Japan) with compression rate of 2 mm/min according to ASTM D 1621-94.

#### 2.4.8 | Real-time FTIR spectroscopy test

Real-time FTIR was performed on a Nicolet MAGNA-IR 750 spectrophotometer (England) equipped with a temperature-controlled heating device. Ground powdery mixtures of sample and KBr were pressed into a tablet and then positioned in a ventilated oven. The heating rate of the oven was 10 °C/min.

#### 2.4.9 | Water resistance test

For the water resistance of flame-retardant RPUF, the samples were soaked in water at 70 °C for 168 h, and then the treated samples were dried at 80 °C to a constant weight. The weight of the samples was measured before water soaking and after drying. The migration percentage was calculated by the Equation 1:

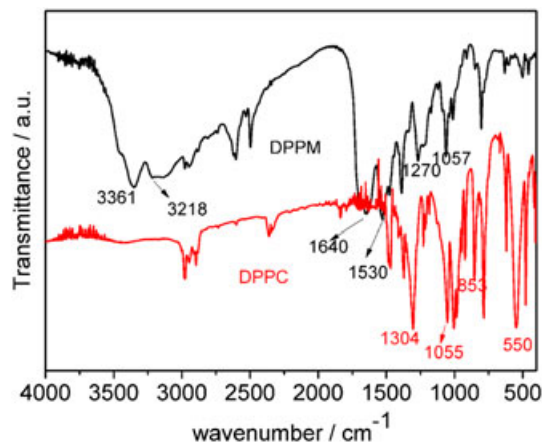
$$\text{Migration Percentage (M)} = \frac{W_0 - W}{W_0} \times 100\% \quad (1)$$

where  $W_0$  is the initial weight of the samples before water soaking, and  $W$  is the remaining weight of the samples after water soaking and drying.

### 3 | RESULTS AND DISCUSSION

Figure 1 shows the FT-IR spectra of DPPC and DPPM. Some characteristic peaks indexed for DPPC: 1304 cm<sup>-1</sup> (P=O), 1055 cm<sup>-1</sup> (P-O-C), 853 cm<sup>-1</sup> (P-O) and 550 cm<sup>-1</sup> (P-Cl) were consistent with those of the literature.<sup>5</sup> DPPM had 2 characteristic absorption peaks at 3361 and 3218 cm<sup>-1</sup>, which were due to the vibration absorption of -NH<sub>2</sub> and =NH, respectively. The characteristic peaks of triazine ring in DPPM were found at 1640 and 1530 cm<sup>-1</sup>. Compared with the peak of 1304 cm<sup>-1</sup> for P=O in DPPC, the stretching vibration of P=O in DPPM fell to 1270 cm<sup>-1</sup> due to the resonant effect between P=O and N, and the disappearance of the peak at 550 cm<sup>-1</sup> (P-Cl) in DPPM. All these verified the successful synthesis of DPPM.

Figure 2 shows the <sup>1</sup>H NMR spectrum of DPPM. The peaks can be assigned as  $\delta = 0.82\text{--}0.94$  ppm (-CH<sub>3</sub>, 6H),  $\delta = 1.08\text{--}1.21$  ppm (C-HCH<sub>2</sub>, 4H),  $\delta = 3.70\text{--}3.73$  ppm (O-CH<sub>2</sub>, 4H),  $\delta = 6.72$  ppm (O = P-NH, 1H) and  $\delta = 7.48\text{--}7.51$  ppm (-NH<sub>2</sub>, 4H). The structure of DPPM was also confirmed by the <sup>24</sup>P NMR spectrum, Figure 3,

**FIGURE 1** FT-IR spectra of DPPM and DPPC [Colour figure can be viewed at [wileyonlinelibrary.com](http://wileyonlinelibrary.com)]

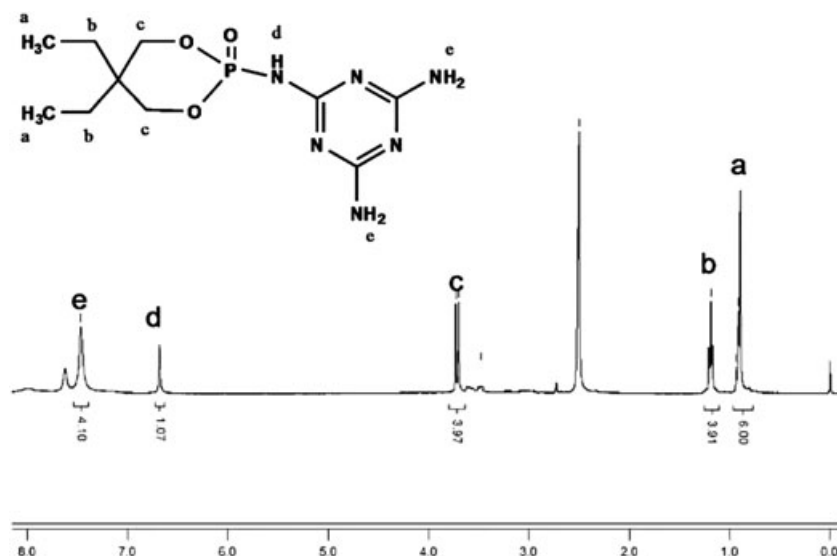


FIGURE 2  $^1\text{H}$  NMR spectrum of DPPM

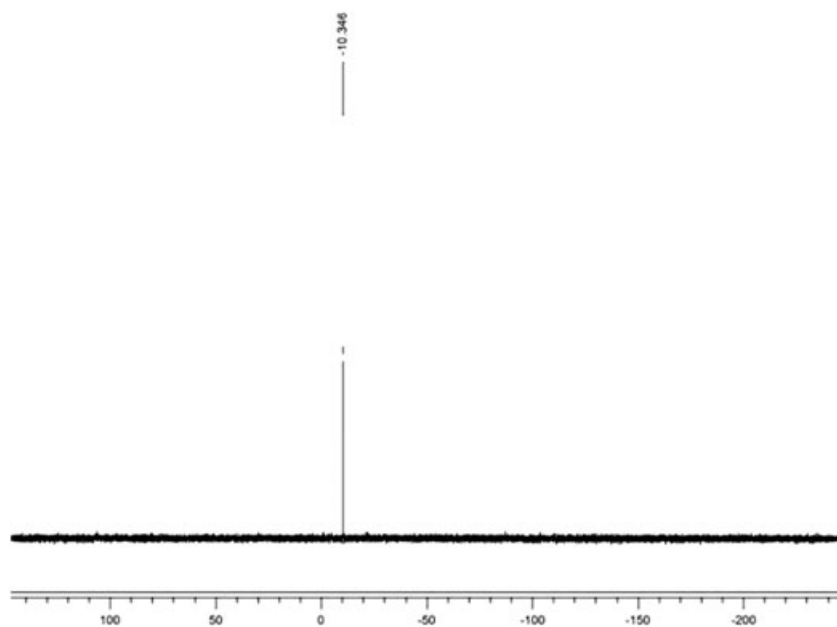


FIGURE 3  $^{24}\text{P}$  NMR spectrum of DPPM

where a sharp signal was observed at  $\delta = -10.35$  ppm, confirming the purity and structure of the compound. The structure of DPPM was further confirmed by elemental analysis. Table 2 shows that the actual content of nitrogen, carbon, and hydrogen was almost coincident with their theoretical contents. On the basis of the above results, it could be concluded that DPPM had been synthesized successfully.

In general, the incorporation of fillers into RPUF caused inferior mechanical properties. For example, for the flame-retardant RPUFs with IFR expandable graphite/ammonium polyphosphate (EG/APP),

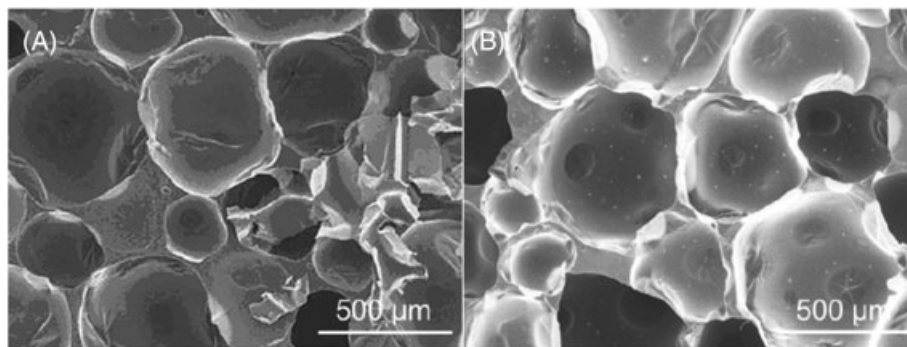
TABLE 2 Actual and theoretical contents of elements in DPPM

	Sample(DPPM)		
	C (%)	H (%)	N (%)
Theoretical content	39.74	6.34	27.80
Actual content	39.53	6.27	27.23

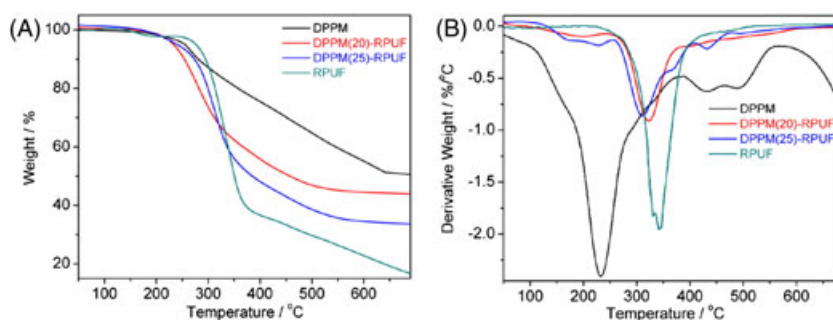
the compressive strength of RPUF was reported to be decreased by 40% when the content of EG/APP was 15 php.<sup>23</sup> The effects of DPPM on the mechanical properties of RPUF are summarized in Table 3. A slight increase in the foam density was observed with increasing the DPPM content, which was probably due to the

TABLE 3 Mechanical properties of RPUF with and without DPPM

Samples	DPPM content (php)	Density (kg/m <sup>3</sup> )	Compress strength (MPa)
RPUF	0	50.3	0.36
DPPM(5)-RPUF	5	52.4	0.34
DPPM(10)-RPUF	10	54.7	0.31
DPPM(15)-RPUF	15	57.0	0.30
DPPM(20)-RPUF	20	58.7	0.28
DPPM(25)-RPUF	25	60.6	0.27



**FIGURE 4** SEM images of (a) RPUF and (b) RPUF filled with 25 php DPPM



**FIGURE 5** TGA (a) and DTG (b) curves of DPPM, RPUF and DPPM-RPUF under  $N_2$  atmosphere [Colour figure can be viewed at [wileyonlinelibrary.com](http://wileyonlinelibrary.com)]

increase of DPPM particles embedded in the cell wall and the decrease of cell volume.<sup>25,26</sup> Meanwhile, the compressive strength of the DPPM(25)-RPUF was only decreased by 25.0% compared to that of pure RPUF, possibly because that the cell structure of the foam containing 25 php DPPM was not destroyed, as shown in Figure 4. The results confirm that DPPM had a favorable compatibility with RPUF.

To investigate the effect of the flame-retardant DPPM on the thermal stability, TGA was carried out and the results were analysed.<sup>27,28</sup> Figure 5 shows the TGA and DTG thermograms. The data are summarized in Table 4. The  $T_{\text{onset}}$  of DPPM was observed to be 253.0 °C and had a residue of 50.5% at 700 °C in  $N_2$ , indicating that DPPM was an efficient char-forming agent. DPPM had a major weight-loss stage at 264.3 °C, which could be assigned to the intumescent chars formation at this temperature.<sup>26</sup> This results indicate that DPPM can be decomposed sharply at high temperatures, and thereby DPPM can also form polyphosphoric acid, which can further accelerate the carbon reaction of RPUF as a dehydrating agent.<sup>27,28</sup> The  $T_{\text{onset}}$  and  $T_{\text{max}}$  of RPUF were 275.2 °C and 342.3 °C, respectively. Compared to the TGA and DTG data of DPPM and

RPUF, the DPPM was degraded earlier than RPUF, and the  $T_{\text{max}}$  was lower than that of RPUF, indicating that DPPM might form intumescent chars and carbon layer by pyrolysis to inhibit RPUF decomposing. This result indicates that DPPM was a suitable flame retardant for RPUF matrix.<sup>1</sup>

Also, only 1-step decomposition was found in the range of 350 °C to 500 °C for RPUF and DPPM-RPUF under  $N_2$ . Compared to the RPUF, the  $T_{\text{onset}}$  of DPPM (20)-RPUF and DPPM(25)-RPUF was lower, which was related to the higher thermal stability of DPPM in this temperature range. The decrease of  $T_{\text{max}}$  was attributed to the decomposition of IFR DPPM and the formation of polyphosphoric acid, which might reduce the reaction activation energy of flame-retardant RPUF as a strong Lewis acid catalyst. This phenomenon was also found in the RPUF containing melamine polyphosphate.<sup>19</sup> At high temperature, DPPM(25)-RPUF had a high char yields, ie, 48.4% at 700 °C, in comparison with the RPUF, ie, 15.1% at 700 °C. The high yield of residual char indicated that DPPM was an effective charring agent. The chars could resist even higher temperatures and shield the underlying polymers from being attacked from oxygen and radiant heat.<sup>29</sup> Therefore, the decomposition loss rate of DPPM (20)-RPUF and DPPM(25)-RPUF was decreased remarkably compared to that of RPUF, and the decomposition rate of DPPM(25)-RPUF was much smaller than that of DPPM (20)-RPUF with increasing the content of DPPM in RPUF. The result demonstrated that the addition of DPPM could enhance effectively the flame retardancy of the RPUF.

In order to evaluate flammability of the DPPM-RPUF, the LOI and UL-94 test results of the RPUF with different mass ratios of DPPM are listed in Table 5. It could be seen that pure RPUF showed low flame retardancy, the LOI value was 17%, and the UL-94 test

**TABLE 4** Data of TGA and DTG thermograms

Samples	$T_{\text{onset}}$ (°C)	$T_{\text{max}}$ (°C)	Residue at 700 °C(%)
DPPM	253.0	264.3	50.5
RPUF	276.0	367.5	15.0
DPPM(20)-RPUF	246.9	322.3	35.6
DPPM(25)-RPUF	233.9	309.7	48.4

$T_{\text{onset}}$ : the 5% weight loss temperature.  $T_{\text{max}}$ : maximum weight loss temperature.

**TABLE 5** LOI and UL-94 results of the samples before and after water soaking

Samples	Before soaking		After soaking		Migration percentages (%)
	LOI	UL 94 rating	LOI	UL 94 rating	
RPUF	17.0	No rating	17.0	No rating	0
DPPM(5)-RPUF	21.5	No rating	19.5	No rating	1.5
DPPM(10)-RPUF	24.5	No rating	23.5	No rating	1.84
DPPM(15)-RPUF	25.5	V-1	25.0	No rating	2.37
DPPM(20)-RPUF	27.5	V-0	26.0	V-0	3.43
DPPM(25)-RPUF	29.5	V-0	28.5	V-0	4.30

**TABLE 6** Cone calorimeter data of RPUF and DPPM(25)-RPUF

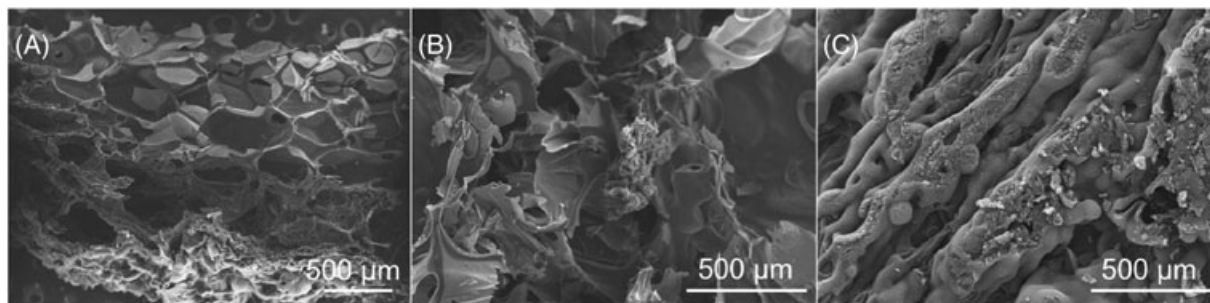
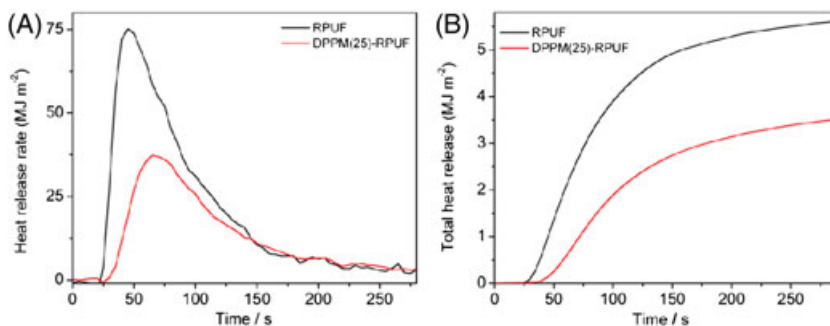
Samples	RPUF	DPPM(25)-RPUF
PHRR, kW/m <sup>2</sup>	75.2	37.3
AHRR, kW/m <sup>2</sup>	22.6	12.5
THR, MJ/m <sup>2</sup>	5.46	3.51

was classified as “no rating.” However, the flame retardancy was significantly improved with further adding DPPM. The LOI of DPPM(25)-RPUF was increased from 17% to 29.5%, and the UL-94 result was classified as “V-0 rating.” The water resistance of the DPPM-RPUF was studied, too. It can be clearly seen that DPPM-RPUF had a very low migration percentage, demonstrating that DPPM had an excellent water resistance. In addition, the water soaking had less impact on the flame retardancy of the DPPM-RPUF. In spite of the slight decline in the LOI values after water treatment, a good maintaining of the UL-94 rating was observed. For instance, the LOI value of DPPM(25)-RPUF was 29.5%, whereas the value

was still as high as 28.5% and the UL-94 test could still obtain a “V-0 rating” after soaking.

The useful information on fire could be provided by cone calorimetry test, which had a good correlation with the real fire disaster. Thus, it was used to predict the behavior of the materials in real fires. It was well known that the heat release rate (HRR) and total heat release (THR) were very important parameters for studying the flammability behavior and could be used to express the fire intensity and fire spread rate.<sup>30</sup> The data and curves of RPUF and DPPM(25)-RPUF by cone calorimeter are shown in Table 6 and Figure 6. The peak HRR (PHRR) of DPPM(25)-RPUF was 37.3 kW/m<sup>2</sup>, with a 50.4% decrease compared with that (75.2 kW/m<sup>2</sup>) of RPUF. In addition, the apparent HRR (AHRR) of DPPM(25)-RPUF was remarkably decreased to 12.5 kW/m<sup>2</sup>, with a 44.4% decrease compared with that (22.5 kW/m<sup>2</sup>) of RPUF. Figure 6 shows the THR for RPUF and DPPM(25)-RPUF. The THR of DPPM(25)-RPUF was observed to be decreased to 3.51 MJ/m<sup>2</sup> from 5.46 MJ/m<sup>2</sup> of RPUF, decreased by 38.3%. The DPPM(25)-RPUF had a lower PHRR, AHRR and THR, which further indicated its excellent flame retardancy.

To further clarify the flame-retardant mechanism, the morphology of the char residues for the DPPM-RPUF was observed. Figure 7 shows the SEM micrographs of the residues for the DPPM(25)-RPUF and RPUF. From the intersection surface of the char from DPPM(25)-RPUF, the outer surface of the char was observed to be compact and smooth; however, the inner surface of the char was loose and existed incompletely burned polyurethane residues, indicating that the outer compact char inhibited effectively the underlying polyurethane to flame. The surface morphology of the char residues of the DPPM(25)-RPUF and RPUF was further observed; there was a compact and continuously swollen char covered on the composites, which effectively prevented both heat and mass transfer. In contrast,

**FIGURE 6** The HRR curves (a) and the THR curves (b) of RPUF and DPPM(25)-RPUF [Colour figure can be viewed at [wileyonlinelibrary.com](http://wileyonlinelibrary.com)]**FIGURE 7** The SEM micrographs of the residues: the intersection surface of the char from (a) DPPM(25)-RPUF, (b) the surface of the char from RPUF, (c) the surface of the char from DPPM(25)-RPUF

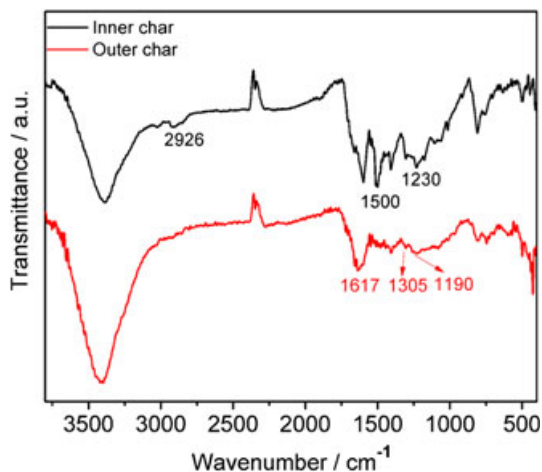


**FIGURE 8** FTIR spectra of the residual char of DPPM(25)-RPUF [Colour figure can be viewed at [wileyonlinelibrary.com](http://wileyonlinelibrary.com)]

the char layer of RPUF was rather incompact and broken up, which might be the reason for its unsatisfied flame-retardant property. Based on the aforementioned information, it could be concluded that the protection mechanism was based on the surface charred layer acting as a physical barrier, which slowed down the decomposition of RPUF and prevented the heat and mass transfer between the gas and the condensed phases.<sup>31</sup>

The compositions of char residues were analyzed. Figure 8 shows the FTIR spectrum of the intumescent residual char for DPPM(25)-RPUF. For the outer char of DPPM(25)-RPUF, the peak at 1617  $\text{cm}^{-1}$  was attributed to the characteristic peak of C=C of aromatic ring, which demonstrated high thermal stability.<sup>32</sup> The characteristic peaks of O=P-O-P=O and O=P-O-C were observed at 1190 and 1305  $\text{cm}^{-1}$ , respectively, indicating the formation of more thermally stable polyphosphate species.<sup>33</sup> The FTIR spectra showed that the polyphosphoric acids might be produced by DPPM in the polyurethane matrix during the thermal degradation, which acted as the dehydration agents and accelerated the formation of heat resistant carbonaceous char, having the characteristics structure of polyaromatic ring by carbonization.<sup>34</sup> For the inner char of DPPM(25)-RPUF, the characteristic peaks of C=C, O=P-O-C and O=P-O-P=O at 1615, 1302 and 1185  $\text{cm}^{-1}$  appear;

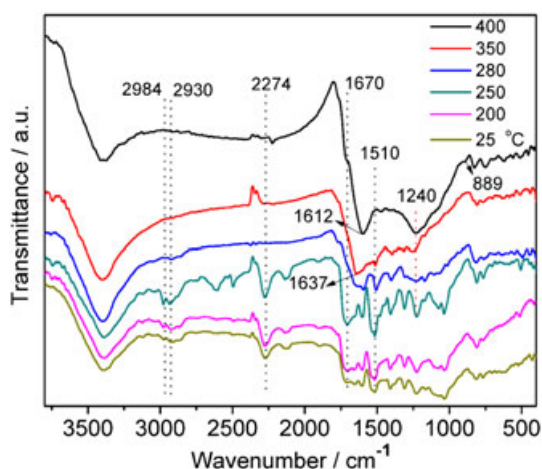


**FIGURE 9** FTIR spectra of DPPM(25)-RPUF at different temperatures [Colour figure can be viewed at [wileyonlinelibrary.com](http://wileyonlinelibrary.com)]

however, the absorption peaks, at 2900 and 1506  $\text{cm}^{-1}$  of C—H and benzene ring in polyurethane were retained, indicating the incompletely burned polyurethane residues. The results further demonstrated that the outer compact char could protect the polyurethane from burning.

To confirm whether the polyphosphoric acids were produced in the thermal degradation of DPPM(25)-RPUF, the thermo-oxidative degradation of DPPM(25)-RPUF was analyzed by real-time FTIR at different temperatures, Figure 9. The characteristic absorption bands of DPPM(25)-RPUF at ambient temperature were displayed in the following: 1510  $\text{cm}^{-1}$ , aromatic absorption band; 1670 and 2730  $\text{cm}^{-1}$ , C=O stretching and symmetrical stretching of isocyanate group; 2930 and 2984  $\text{cm}^{-1}$ , asymmetrical stretching of —CH<sub>2</sub> and —CH<sub>3</sub>.<sup>35</sup> Although all of these peaks were visible at ambient temperature, the intensity of these peaks decreased with increasing the temperature and almost disappears at 280 °C, indicating the thermal degradation of DPPM(25)-RPUF. The characteristic absorption peaks of DPPM could not be clearly detected at ambient temperature. This is possibly because that the content of DPPM was very low in RPUF so that the characteristic absorption peaks were overlapped with the characteristic bands of RPUF. In particular, the band of P=O in the pyrophosphate was observed at 1240  $\text{cm}^{-1}$  at 350 °C and the appearance of a peak at 889  $\text{cm}^{-1}$  at 400 °C, which should be assigned to the asymmetric stretching vibration of P-O-P.<sup>34</sup> This indicates that more polyphosphate species were produced from the condensation reaction of pyrophosphate. With the increase of temperature, the presence of polyphosphates could promote the formation of highly structured char. Some unsaturated compounds were formed according to the new wide peaks at about 1637  $\text{cm}^{-1}$  corresponding to the stretching vibration of C=C bond at 350 °C. With further increasing the temperature, the absorption band of C=C was observed at 1612  $\text{cm}^{-1}$ , indicating the possible reorganization of carbon atoms in C=C into aromatic species.<sup>35</sup>

## 4 | CONCLUSIONS

A novel phosphorus-nitrogen single IFR, 2,2-diethyl-1,3-propanediol phosphoryl melamine (DPPM), was synthesized and well characterized. DPPM exhibited a favorable compatibility with RPUF and a negligibly negative influence on the mechanical properties of RPUF. Particularly, DPPM exhibited excellent flame retardancy performance and outstanding water resistance in RPUF. TGA results showed that the onset decomposing temperature of the DPPM-RPUF decreased but the char yields increased. The SEM and FTIR results indicated that the flame-retardant mechanism of DPPM in RPUF was the forming of intact and continuous char layer on the surface of RPUF in thermal degradation of the composite, which prevented the heat and mass transfer between the gas and the condensed phases and effectively protected the substrate material from burning. These flame retardants can be extended for multifunctional polymer nanocomposites with an aim to broaden the applications of inert polymers especially in the form states in the fields such as electromagnetic interference shielding,<sup>36-38</sup> energy storage<sup>39</sup> and other sensing applications.<sup>40-49</sup>

## ACKNOWLEDGMENTS

This research is financially supported by the National Natural Science Foundation of China (No. 51603194), North University of China (NUC), and start-up funds from University of Tennessee. Dr. Z. Wang would like to thank the supports from the NIMHD-RCMI grant number 5G12MD007595 from the National Institute on Minority Health and Health Disparities and the NIGMS-BUILD grant number 8UL1GM118967.

## REFERENCES

- Chen X, Huo L. TG-FTIR characterization of volatile compounds from flame retardant polyurethane foams materials. *J Anal Appl Pyrol.* 2013;100:186-191.
- Gu H, Mao C, Gu J, Guo Z. An overview of multifunctional epoxy nanocomposites. *J Mat Chem C.* 2016;4:5890-5906.
- Yang C, Wei H, Guan L, Guo Z. Polymer nanocomposites for energy storage, energy saving, and anticorrosion. *J Mat Chem A.* 2015;3:14929-14941.
- Wei H, Cui D, Guo Z. Energy conversion technologies towards self-powered electrochemical energy storage systems: The state of the art and perspectives. *J Mat Chem A.* 2017;5:1873-1894.
- Zhang Y, Shang S, Zhang X, Wang D, Hourston DJ. Impact modification of aromatic/aliphatic polyamide blends: Effects of composition and processing conditions. *J Appl Polym Sci.* 1996;59:1167-1177.
- Goods SH, Neuschwanger CL, Henderson CC, Skala DM. Mechanical properties of CRETE, a polyurethane foam. *J Appl Polym Sci.* 1998;68:1045-1055.
- Cunningham RL, Gordon SH, Felker FC, Eskins K. Glycols in polyurethane foam formulations with a starch-oil composite. *J Appl Polym Sci.* 1998;69:957-964.
- Hobbs ML, Erickson KL, Chu TY. Modeling decomposition of unconfined rigid polyurethane foam. *Polym Degrad Stab.* 2000;69:47-56.
- Edward DW, Sergei VL. Commercial flame retardancy of polyurethanes. *J Fire Sci.* 2004;22:183
- Modesti M, Lorenzetti A. Improvement on fire behaviour of water blown PIR-PUR foams: use of an halogen-free flame retardant. *Eur Polym J.* 2003;39:263-268.
- Chen X, Wu H, Zhu L, Yang B, Guo S, Yu J. Synergistic effects of expandable graphite with magnesium hydroxide on the flame retardancy and thermal properties of polypropylene. *Poly Eng Sci.* 2007;47:1756-1760.
- Zheng Y, Zheng Y, Yang S, et al. Esterification synthesis of ethyl oleate catalyzed by Brønsted acid-surfactant-combined ionic liquid. *Green Chem Lett Rev.* 2017;10:202-209.
- Gong T, Liu M, Yang W, et al. Selective distribution and migration of carbon nanotubes enhanced electrical and mechanical performances in polyolefin elastomers. *Polymer.* 2017;110:1-11.
- Liu H, Dong M, Liu C, et al. Lightweight conductive graphene/thermoplastic polyurethane foams with ultrahigh compressibility for piezoresistive sensing. *J Mater Chem C.* 2017;5:73-83.
- Zhao P, Liu S, Xiong K, Wang W, Liu Y. Highly flame retardancy of cotton fabrics with a novel phosphorus/nitrogen/silicon flame-retardant treating system. *Fib Polym.* 2016;17:569-575.
- Li X, Chen H, Wang W, et al. Synthesis of a formaldehyde-free phosphorus-nitrogen flame retardant with multiple reactive groups and its application in cotton fabrics. *Polym Degrad Stab.* 2015;120:193-202.
- Tao K, Li J, Xu L, et al. A novel phosphazene cyclomatrix network polymer: Design, synthesis and application in flame retardant polylactide. *Polym Degrad Stab.* 2011;96:1248-1254.
- Modesti M, Lorenzetti A, Simioni F, Checchin M. Influence of different flame retardants on fire behaviour of modified PIR/PUR polymers. *Polym Degrad Stab.* 2001;74:475-479.
- Thirumal M, Khastgir D, Nando GB, Naik YP, Singha NK. Halogen-free flame retardant PUF: Effect of melamine compounds on mechanical, thermal and flame retardant properties. *Polym Degrad Stab.* 2010;95:1138-1145.
- Duan L, Yang H, Song L, et al. Hyperbranched phosphorus/nitrogen-containing polymer in combination with ammonium polyphosphate as a novel flame retardant system for polypropylene. *Polym Degrad Stab.* 2016;134:179-185.
- Qian X, Lei S, Yuan B, et al. Organic/inorganic flame retardants containing phosphorus, nitrogen and silicon: Preparation and their performance on the flame retardancy of epoxy resins as a novel intumescent flame retardant system. *Mater Chem Phys.* 2014;143:1243-1252.
- Gao M, Wu W, Liu S, Wang Y, Shen T. Thermal degradation and flame retardancy of rigid polyurethane foams containing a novel intumescent flame retardant. *J Therm Anal Calorim.* 2014;117:1419-1425.
- Meng XY, Ling Y, Zhang XG, et al. Effects of expandable graphite and ammonium polyphosphate on the flame-retardant and mechanical properties of rigid polyurethane foams. *J Appl Polym Sci.* 2009;114:853-863.
- Ma Y, Dai J, Wu L, Fang G, Guo Z. Enhanced anti-ultraviolet, anti-fouling and anti-bacterial polyelectrolyte membrane of polystyrene grafted with trimethyl quaternary ammonium salt modified lignin. *Polymer.* 2017;114:113-121.
- Thirumal M, Khastgir D, Singha NK, Manjunath BS, Naik YP. Effect of foam density on the properties of water blown rigid polyurethane foam. *J Appl Polym Sci.* 2008;108:1810-1817.
- König A, Kroke E. Methyl-DOPO—a new flame retardant for flexible polyurethane foam. *Polym Adv Technol.* 2011;22:5-13.
- Camino G, Martinasso G, Costa L. Thermal degradation of pentaerythritol diphosphate, model compound for fire retardant intumescent systems: Part I—Overall thermal degradation. *Polym Degrad Stab.* 1990;27:285-296.
- Camino G, Martinasso G, Costa L. Thermal degradation of pentaerythritol diphosphate, model compound for fire retardant intumescent systems: Part II—Intumescence step. *Polym Degrad Stab.* 1990;28:17-38.
- Ma H, Tong L, Xu Z, Fang Z, Jin Y, Lu F. A novel intumescent flame retardant: Synthesis and application in ABS copolymer. *Polym Degrad Stab.* 2007;92:720-726.
- Wang G, Chen X, Liu P, Bai S. Flame-retardant mechanism of expandable polystyrene foam with a macromolecular nitrogen-phosphorus intumescent flame retardant. *J Appl Polym Sci.* 2017;134:44356-44443.
- Zhan J, Song L, Nie S, Hu Y. Combustion properties and thermal degradation behavior of polylactide with an effective intumescent flame retardant. *Polym Degrad Stab.* 2009;94:291-296.
- Ye L, Wu Q, Qu B. Photocrosslinking and related properties of intumescent flame-retardant LLDPE/EVA/IFR blends. *Polym Adv Technol.* 2012;23:858-865.
- Qu B, Xie R. Intumescent char structures and flame-retardant mechanism of expandable graphite-based halogen-free flame-retardant linear low density polyethylene blends. *Polym Inter.* 2003;52:1415-1422.
- Dai K, Song L, Yuen RK, et al. Enhanced properties of the incorporation of a novel reactive phosphorus- and sulfur-containing flame-retardant monomer into unsaturated polyester resin. *Ind Eng Chem Res.* 2012;51:15918-15926.
- Liu W, Chen DQ, Wang YZ, Wang DY, Qu MH. Char-forming mechanism of a novel polymeric flame retardant with char agent. *Poly Degrad Stab.* 2007;92:1046.
- Guo J, Song H, Liu H, et al. Polypyrrole-interface-functionalized nanomagnetite epoxy nanocomposites as electromagnetic wave absorber with enhanced flame retardancy. *J Mater Chem C.* 2017;5:5334-5344.
- Zhang K, Yu H, Shi Y, et al. Morphological regulation improved electrical conductivity and electromagnetic interference shielding in poly(L-

- lactide)/poly( $\epsilon$ -caprolactone)/carbon nanotubes nanocomposites via constructing stereocomplex crystallites in poly(L-lactide) phase. *J Mat Chem C*. 2017;5:2807-2817.
38. Li J, Liu H, Guo J, et al. Flexible, conductive, porous, fibrillar polymer-gold nanocomposites with enhanced electromagnetic interference shielding and mechanical properties. *J. Mat. Chem. C*. 2017;5:1095-1105.
39. Zheng Y, Zheng Y, Yang S, et al. Esterification synthesis of ethyl oleate catalyzed by Brønsted acid-surfactant-combined ionic liquid. *Green Chem Lett Rev*. 2017; in press. <https://doi.org/10.1080/17518253.2017.1342001>
40. Sun Z, Zhang L, Dang F, Yerra N, Guo Z. Experimental and simulation-based understanding of morphology controlled barium titanate nanoparticles under co-adsorption of surfactants. *CrystEngComm*. 2017;19:3288-3298.
41. Wang M, Zhang K, Dai X, et al. Enhanced electrical conductivity and piezoresistive sensing in multi-wall carbon nanotubes/polydimethylsiloxane nanocomposites via the construction of a self-segregated structure. *Nanoscale*. 2017; in press. <https://doi.org/10.1039/C7NR02322G>
42. Liu H, Dong M, Guo Z. Lightweight conductive graphene/thermoplastic polyurethane foams with ultrahigh compressibility for piezoresistive sensing. *J Mat Chem C*. 2017;5:73-83.
43. Liu H, Gao J, Huang W, et al. Electrically conductive strain sensing polyurethane nanocomposites with synergistic carbon nanotubes and graphene bifillers. *Nanoscale*. 2016;8:12977-12989.
44. Guan X, Zheng G, Dai K, Liu C. Carbon nanotubes-adsorbed electrospun PA66 nanofiber bundles with improved conductivity and robust flexibility. *ACS Appl Mater Interf*. 2016;8:14150-14159.
45. Liu H, Huang W, Gao J, Guo Z, Liu C. Piezoresistive behavior of porous carbon nanotube-thermoplastic polyurethane conductive nanocomposites with ultrahigh compressibility. *Appl Phys Lett*. 2016;108:011904.
46. Jin H, Chen Q, Chen Z, Hu Y, Zhang J. Multi-LeapMotion sensor based demonstration for robotic refine tabletop object manipulation task. *CAAI Transac Intellig Technol*. 2016;1:104-113.
47. Zhang X, Gao H, Guo M, Li D. A study on key technologies of unmanned driving. *CAAI Transac. Intellig Technol*. 2016;1:4-13.
48. Alippi C. A unique timely moment for embedding intelligence in applications. *CAAI Trans Intellig Technol*. 2016;1:1-3.
49. Padhy S, Panda S. A hybrid stochastic fractal search and pattern search technique based cascade PI-PD controller for automatic generation control of multi-source power systems in presence of plug in electric vehicles. *CAAI Trans Intellig Technol*. 2017;2:12-25.

**How to cite this article:** Wang C, Wu Y, Li Y, et al. Flame-retardant rigid polyurethane foam with a phosphorus-nitrogen single intumescent flame retardant. *Polym Adv Technol*. 2018;29:668-676. <https://doi.org/10.1002/pat.4105>